Time-resolved analyses of elemental distribution and concentration in living plants: An example using manganese toxicity in cowpea leaves

F. Pax C. Blamey[1], David J. Paterson[2], Adam Walsh[2], Nader Afshar[2], Brigid A. McKenna[1], Miaomiao Cheng[3], Caixian Tang[3], Neal W. Menzies[1], and Peter M. Kopittke[1]*

[1]The University of Queensland, School of Agriculture and Food Sciences, St. Lucia, Queensland 4072, Australia; [2]Australian Synchrotron ANSTO, Clayton, Victoria 3168, Australia; [3]La Trobe University, Centre for AgriBioscience, Bundoora, Victoria 3086, Australia.

Author for correspondence:
Peter M. Kopittke
Tel: +61 7 3346 9149
Email: p.kopittke@uq.edu.au

Word count:

Summary:	191
Introduction:	931
Materials and Methods:	1902
Results:	1356
Discussion:	1140
Conclusion:	181
Acknowledgements:	68
Total word count (above sections):	**5769**

Number of figures: 6 (plus 3 in Supporting Information)
Figures in color: 1, 2, 3, 4, 5, (plus 3 in Supporting Information)
Number of tables: 0 (plus 1 in Supporting Information)

Summary

- Knowledge of elemental distribution and concentration within plant tissues is crucial in the understanding of almost every process that occurs within plants. However, analytical limitations have hindered the microscopic determination of changes over time in the location and concentration of nutrients and contaminants in living plant tissues.
- We developed a novel method using synchrotron-based micro X-ray fluorescence (μ-XRF) that allows for laterally-resolved, multi-element, kinetic analyses of plant leaf tissues *in vivo*. To test the utility of this approach, we examined changes in the accumulation of Mn in unifoliate leaves of 7-d-old cowpea (*Vigna unguiculata*) plants grown for 48 h at 0.2 and 30 μM Mn in solution.
- Repeated μ-XRF scanning did not damage leaf tissues demonstrating the validity of the method. Exposure to 30 μM Mn for 48 h increased the initial number of small spots of localized high Mn and their concentration rose from 40 to 670 mg Mn kg^{-1} fresh mass. Extension of the two-dimensional μ-XRF scans to a three-dimensional geometry provided further assessment of Mn localization and concentration.
- This method shows the value of synchrotron-based μ-XRF analyses for time-resolved *in vivo* analysis of elemental dynamics in plant sciences.

Key words: cowpea, ionomics, manganese, micro X-ray fluorescence, synchrotron

Introduction

The concentration and distribution of nutrients and contaminants within plant tissues change over time in response to physiological stimuli, developmental stage, and changes in the broader external environment. To understand the underlying genetic and physiological processes influencing plant growth, it is necessary to determine the concomitant changes in the accumulation or decline of these elements within plant tissues. In this regard, ionomics is concerned with the examination of elements in plants, although measurements are normally conducted for bulk tissues (Salt *et al.*, 2008). Whilst such analyses provide valuable information, it is even more useful to determine laterally resolved concentrations of essential and non-essential elements within plant tissues (Conn & Gilliham, 2010). Besides its relevance in plant nutrition, ionomics involves the functional analysis of genes that directly and indirectly control plant development and physiology (Salt *et al.*, 2008; Takahashi *et al.*, 2009).

Various techniques exist for examining the distribution of elements within plant tissues but most techniques require extensive processing of sequential samples. Hence, they are not able to examine nutrient and contaminant changes over time in the same area of living plants. For example, conventional scanning electron microscopy coupled with energy-dispersive X-ray spectroscopy (SEM-EDS) needs an ultra-high vacuum that requires samples to be dehydrated; frozen samples may be used where a cryo-SEM-EDS is available (Cosio *et al.*, 2005). It is perhaps possible to examine living plants using environmental SEM (ESEM), but there are problems with sample size restrictions, electron beam damage, and a comparatively poor detection limit (Danilatos, 1981; McGregor & Donald, 2010). Though having excellent subcellular resolution, nanoscale secondary ion mass spectrometry (NanoSIMS) analysis also requires ultra-high vacuum (Moore *et al.*, 2014). Confocal microscopy with fluorophores is potentially of use for the kinetic analyses of living plants (Walczysko *et al.*, 2000; Babourina & Rengel, 2009) but there are limits imposed by the availability of fluorophores and uncertainty in their selectivity and cellular penetration. Laser ablation inductively coupled plasma mass spectrometry (LA-ICP-MS) is also capable of examining living plants in ambient conditions (Salt *et al.*, 2008) but damage through ablation of the sample surface prevents kinetic analysis of the same tissue area. Autoradiography has been used for the study of plants since the 1920s (Hevesy, 1923), and macro-autoradiography can potentially be used for kinetic analyses of living plants but is limited by poor resolution, long exposure times, limited availability of suitable isotopes, and safety considerations (Solon *et al.*, 2010). Recently-developed radioisotope tracer techniques for *in vitro* analysis, such as a positron-emitting tracer imaging system (Tsukamoto *et al.*, 2006) and magnetic resonance imaging (Jahnke *et al.*, 2009), have overcome some limitations, but it is only possible to examine a single element at a time (Sugita *et al.*, 2016).

Synchrotron-based micro-X-ray fluorescence spectroscopy (μ-XRF) is of interest as there are no theoretical restrictions on sample size, analyses are conducted at ambient temperature and pressure

92 often at a resolution of *c.* ≤ 1 μm with a detection limit of *c*. 0.1 to 100 mg kg^{-1} fresh mass (FM). Leaf
93 tissues of living plants may be examined also (Scheckel *et al.*, 2004). Depending upon the element of
94 interest and beamline specifications, this technique can simultaneously generate maps for multiple
95 elements within the energy range of the beamline, often 2 to 25 keV allowing analysis from P to Ag at
96 the K-edge. Early analyses of plant tissues using μ-XRF analyses focused on dehydrated tissues of
97 hyperaccumulators (McNear *et al.*, 2005; McNear & Küpper, 2014). However, tissue dehydration
98 may result in experimental artifacts and the high concentrations used in studies of hyperaccumulators
99 are not relevant to many crop species. With progressive improvements in technology (specifically, the
100 development of more efficient fluorescent X-ray detectors), there has been increasing interest in the
101 analysis of hydrated tissues of non-hyperaccumulating species (Lombi *et al.*, 2011a; Blamey *et al.*,
102 2015; Kopittke *et al.*, 2015). For example, studies of Cu, Ni, Zn, and Mn rhizotoxicity in hydrated
103 cowpea (*Vigna unguiculata*) roots showed Cu located in the rhizodermis and outer cortex, Ni in the
104 inner cortex, and Zn in the stele; the meristematic zone was high in both Zn and Mn (Kopittke *et al.*,
105 2011; Kopittke *et al.*, 2013). However, problems may still arise with radiation damage and leaf tissue
106 dehydration by high-energy X-rays upon repeated scanning of the same area of leaf (Lombi & Susini,
107 2009) that would preclude repeated analysis of living tissues.
108 To examine the potential of synchrotron-based μ-XRF for the analysis of living plants, we
109 inspected changes in element distribution in leaves of cowpea following exposure to an adequate and
110 a toxic level of Mn in the rooting medium. Using μ-XRF, we previously identified high Mn in
111 sunflower (*Helianthus annuus*) trichomes and in vacuoles of white lupin (*Lupinus albus*) as
112 mechanisms of tolerance (Blamey *et al.*, 2015). Such mechanisms are not present in cowpea (an
113 established model species in Mn toxicity studies) and soybean (*Glycine max*), making these crop
114 species considerably more sensitive to high Mn^{2+} in the root environment that results from the
115 localized accumulation of Mn in leaf tissues (Heenan & Carter, 1976; Horst, 1983). The first visible
116 symptom of toxicity is the appearance of small dark spots on unifoliate leaves *c.* 4-d after exposure of
117 roots to 20 μM Mn (Wissemeier & Horst, 1987). Thus, the present study tested the suitability of μ-
118 XRF for *in situ*, multi-element, kinetic, microscopic analyses to quantify changes in elemental
119 distribution in leaves of living cowpea plants. We envisage that the method developed here will be of
120 importance across a wide range of studies for the examination of plant responses to physiological
121 stimuli, developmental stage, and changes in biotic and abiotic environments.
122
123 **Materials and Methods**
124
125 **Plant growth**
126
127 Cowpea (*Vigna unguiculata* L. Walp. cv. Bunya) seeds in rolled paper towels were placed in tap
128 water and seedlings transplanted 4 d later into 20 L of aerated nutrient solution at pH 5.6 and ionic

129 strength of *c.* 3 mM (Blamey *et al.*, 2015) approximating that in soil solutions (Kopittke *et al.*, 2010).
130 Nominal concentrations of nutrients in the basal solution were (μM): 1000 Ca, 120 NH_4^+-N, 95 Mg,
131 300 K, 10 Na, 6 Fe, 0.2 Mn, 0.5 Zn, 0.2 Cu, 1250 Cl, 670 NO_3^- -N, 340 S, 5 P, 1 B, and 0.01 Mo.
132 After 7 d in a controlled environment room at 25 °C under fluorescent lights, plants were transferred
133 to the Australian Synchrotron and grown in fresh nutrient solutions at 22 °C under high-pressure
134 sodium lights at photosynthetically active radiation (PAR) of 1,500 μmol m^{-2} s^{-1}. Mean
135 concentrations of selected nutrients measured by inductively coupled optical emission spectroscopy
136 (ICP-OES) in solutions at the beginning and end of the initial and final periods were (μM): 1,050 Ca,
137 120 Mg, 360 K, 30 Na, 0.23 Mn, 10 Fe, 0.4 Zn, 0.2 Cu, 360 S, 7 P, and 4 B. Use of 15 % NH_4^+-N in
138 solution ensured that the initial solution pH 5.6 did not require adjustment.
139 A preliminary experiment tested if repeated μ-XRF scans (see below) of the same area of leaf
140 caused damage that would potentially modify the transport of solutes in the xylem and phloem or
141 cause other experimental artifacts (e.g. dehydration). This involved excision of a unifoliate leaf
142 followed by mounting between two layers of 4-μm Ultralene® film on a specimen holder that
143 provided support and limited dehydration (Fig. 1a).
144 The main experiment involved the transfer of four plants, each to a 50-mL polypropylene
145 centrifuge tube (30 × 115 mm) with roots submerged in 40 mL of basal nutrient solution. Securing the
146 plant stem in the neck of the tube by rolling a length of 15-mm wide geotextile covered by a slotted
147 cap and Parafilm M® prevented spillage onto sensitive equipment. Also secured in the neck of the
148 centrifuge tube were two 2-m lengths of PTFE #2 AWG thin-wall tubing (Cole-Parmer Instrument
149 Company, Vernon Hills IL, USA), one serving as solution input and the other as output. Tygon®
150 tubing with 0.7-mm internal diameter joined the PTFE tubing where necessary. The input tube
151 connected a 10-L reservoir of continuously aerated nutrient solution via a four-roller peristaltic pump
152 to the bottom of the solution in the centrifuge tube. The output tube extended from the 40-mL mark of
153 the centrifuge tube to the reservoir via the peristaltic pump, adjustment of which ensured no solution
154 overspill. Circulation of nutrient solution between the reservoir and the centrifuge tube at a measured
155 rate of 4 mL min^{-1} enabled 90 % renewal of the 40 mL of nutrient solution in < 30 min. Two purpose-
156 built sample holders, each with two centrifuge tubes, contained plants fixed to each holder. Securing a
157 unifoliate leaf of each plant with Ultralene® and double-sided tape protected the sensitive Be detector
158 window *c.* 1 mm away but also allowed transpiration via both the adaxial and abaxial leaf surfaces
159 (Fig. 2a). Each sample holder (i.e. replicate) with two secured plants was attached in turn to the
160 sample stage that allowed horizontal and vertical adjustment of the leaves and correct focusing of the
161 X-ray beam (Fig. 2b). With solution in each centrifuge tube connected to a 10 L-reservoir, we
162 imposed two treatments with nominal 0.2 (i.e. basal) and 30 μM Mn. Mean measured values at the
163 start and end of the 48-h experimental period were 0.33 and 30 μM Mn.
164 An important objective of the main experiment was ensuring optimal plant growth conditions
165 other than in the 30 μM Mn treatment. We had initially intended to renew the 40 mL of solution in

166 each centrifuge tube at appropriate intervals, but an anticipated rapid decrease in dissolved O_2
167 precluded this approach. Specifically, we calculated that a 7-d-old root system (2.5 g FM plant^{-1}) with
168 an O_2 consumption rate of 20 µmol g^{-1} FM h^{-1} (Bravo & Uribe, 1981) would deplete the 510 µmol
169 dissolved O_2 in 40 mL solution at 25 °C in < 30 min. Thus, root O_2 and nutrient requirements over 48
170 h were met by circulating 10 L of aerated solution. Use of a peristaltic pump and reservoirs placed on
171 the floor proved satisfactory provided the outflow rate exceeded that of the inflow to prevent overflow
172 of the 50-mL centrifuge tube. This ensured the safety of sensitive electronic equipment that had
173 previously been avoided through use of solid growth medium (Scheckel *et al.*, 2004) or a small
174 reservoir of solution with *Arabidopsis thaliana* plants (Fittschen *et al.*, 2017). Additionally, we had to
175 prevent damage to the fragile Be window of the Maia detector despite the need for unifoliate leaves
176 being at a distance of *c.* 1 mm for correct focus (http://www.synchrotron.org.au/aussyncbeamlines/x-
177 ray-fluorescence-microscopy/samples). Securing the unifoliate leaves to the sample holder with
178 Ultralene® and double-sided tape (Fig. 2a) and moving the other leaves away from the detector (Fig. 2
179 b) overcame this potential problem.
180 The final experiment of this study determined the bulk concentration of Mn in unifoliate
181 leaves of cowpea plants grown in a laboratory under high-pressure sodium lights at 25 °C using the
182 same procedure as above. Four plants in each of six 20-L pots were grown in basal nutrient solution
183 for 7 d after transplanting at which time three replicates of 0.2 and 30 µM Mn were imposed for 2 d.
184 Mean concentrations of selected nutrients in solution measured by ICP-OES were (µM): 820 Ca, 85
185 Mg, 50 K, 20 Na, 10 Fe, 0.28 Zn, 0.12 Cu, 150 S, 10 P, and 2.7 B. The mean concentration of Mn was
186 0.23 and 28 µM in the two treatments at the start and end of 2 d. Four unifoliate leaves were harvested
187 from each pot, FM and dry mass (DM) determined, and leaves digested in 5:1 HNO_3:$HClO_4$ prior to
188 Mn analysis using ICP-OES.
189
190 **µ-XRF scans**
191
192 Details of the XFM beamline at the Australian Synchrotron have been provided by Paterson
193 *et al*. (2011), as have details for the analysis of fresh hydrated roots by Kopittke *et al*. (2011) and
194 leaves by Blamey *et al*. (2015). X-rays, at an energy of 12.9 keV in the present study, were selected
195 using a Si(111) monochromator and focused (2 × 2 µm) by a pair of Kirkpatrick-Baez mirrors and the
196 X-ray fluorescence emitted by the specimen collected in a backscatter geometry using a 384-element
197 Maia detector system (Lombi *et al.*, 2011a; Paterson *et al.*, 2011). Elemental mapping is conducted
198 on-the-fly in the horizontal direction. Until recently, discrete steps in the vertical direction increased
199 the dwell at the edge of the scanned area (i.e. at the end of each horizontal line scan) with greater
200 potential for X-ray damage to hydrated tissues. A recent improvement allows significantly faster and
201 more accurate raster scanning via kinematically optimized fly-scans known as Rascan, a system that
202 wraps the motion controller into an optimal two-dimension scanner. This device renders a motion

203 trajectory optimized for smoothness, as well as minimal overhead times, for a given fly-scan of
204 known transit time (dwell) and pitch. Importantly, Rascan reduces end-of-line overheads from > 350
205 ms to *c*. 35 ms resulting in a *c*. 30 % reduction in scan time and less radiation damage. Using this
206 approach, analyses are routinely conducted with a dwell of ≤ 1 ms $pixel^{-1}$, comparing favorably to
207 many other synchrotron-based μ-XRF beamlines where a dwell of 10 to 100 ms $pixel^{-1}$ is common
208 (Lombi *et al.*, 2011b). This decreased dwell using the Maia detector system and Rascan at the
209 Australian Synchrotron facilitated the present study with repeated scanning of the same area of living
210 plant leaf tissues.
211 The preliminary experiment determined if sequential scanning of the same area resulted in
212 damage from high energy X-rays. The survey scan started within 5 min of excising and mounting a
213 unifoliate leaf (Fig. 1a) and took 52 min to complete an area of 47 × 33 mm with a step size (i.e.
214 virtual pixel size) of 50 μm. From this survey scan, a 7 × 3 mm area was selected for further
215 examination with three detailed scans with a step size of 5 μm, each scan taking *c*. 20 min. Each of
216 the detailed scans covered a slightly larger area encompassing the entire previous scan to test if the X-
217 rays damaged the leaf that would be evident in the subsequent scans by changes in sample hydration
218 and elemental redistribution. A fourth, high-resolution scan with a step size of 2 μm covering an area
219 of 1.54 × 0.79 mm tested the possibility of damage in detail. We also used light microscopy to
220 examine the leaf for any visible signs of damage.
221 Thereafter, the main experiment involved securing the sample holder with two centrifuge
222 tubes, each with a living plant (Fig. 2), in the beamline and verifying basal solution (0.2 μM Mn) flow
223 rate. Addition of a 0.46-mL aliquot of 0.65 M $MnSO_4$ stock solution to one of the 10-L reservoirs
224 imposed a 30-μM Mn treatment. Two initial survey scans of 6 and 2 min identified the area for
225 detailed scans (Fig. 2c), the first of which started immediately thereafter (0 h). This and subsequent
226 detailed scans took *c.* 120 min to complete. There were six scans from 0-2, 6-8, 12-14, 18-20, 24-26,
227 and 48-50 h after first imposition of Mn treatments. The same procedures and scans of adjacent
228 unifoliate leaves followed with living plants in the second replicate. In the replicate reported here, the
229 detailed scan area was *c.* 120 mm^2, which included a leaf area of 55.2 and 56.4 mm^2 in the 0.2 and 30
230 μM Mn treatments. The detailed scans had 4 × 4 μm pixels and a velocity of 4 mm s^{-1} resulting in a
231 pixel transit time of 1 ms. With a total photon flux of *c*. 2×10^9 photon s^{-1} at an energy of 12.9 keV,
232 these scan parameters corresponded to *c*. 1.3×10^5 photon μm^{-2} for each scan (i.e. a total of 8.0×10^5
233 photon μm^{-2} for the six scans).
234 On completion of the scans, the CSIRO Dynamic Analysis method in GeoPIXE provided
235 quantitative, true-element images of X-ray fluorescence spectra (Ryan & Jamieson, 1993; Ryan,
236 2000) as outlined at http://www.nmp.csiro.au/dynamic.html. The survey scans required correction for
237 variation in leaf thickness arising from the major leaf veins by normalizing to Compton scatter.
238 Sections of leaves for detailed scans had only a few minor veins (Fig. 2c) that did not interfere greatly

239 with determination of the two-dimensional areal concentrations of elements and their distributions
240 (Kopittke *et al.*, 2011).
241 GeoPIXE provided initial quantitative analysis of Mn concentration in 2.6 × 0.08 mm
242 transects of detailed scans across the leaf at 30 μM Mn from 0 to 48 h that involved 650 individual
243 pixels in the horizontal direction × the mean of 20 pixels in the vertical direction. This was followed
244 by determining Mn in the high-resolution image area of 2.6 × 0.6 mm (i.e. values of individual 650 ×
245 150 pixels). Further analysis using GeoPIXE and ImageJ 1.48v (Schneider *et al.*, 2012) extended the
246 two-dimension μ-XRF scans to a three-dimensional geometry of Mn distribution and concentration.
247 The number and localized areas of Mn accumulation and the distributions of K, Ca, Fe, Cu, and Zn at
248 0 and 48 h in the two Mn treatments were determined also.
249
250 **Results**
251
252 **Potential X-ray damage to living unifoliate leaves**
253
254 The Australian Synchrotron XFM beamline Maia detector system with fast data acquisition has the
255 advantage of rapid pixel transit times (Paterson *et al.*, 2011) but sequential *in situ* μ-XRF analyses of
256 hydrated leaf tissues may still result in radiation damage and tissue dehydration as shown in micro-
257 tomography of a cowpea root (Lombi *et al.*, 2011a). This was evident also in an unpublished study
258 using X-ray absorption near edge structure (XANES) imaging of a 4.0 × 2.5 mm section of a soybean
259 leaf at high Mn with repeated scans of the same area at increasing energy. Compared to the rest of the
260 leaf, the rectangular scanned area was mildly chlorotic suggestive of radiation damage (Fig. S1a).
261 Furthermore, there were changes in the distribution of Ca (Fig. S1b) and dehydration damage evident
262 in Compton scatter (Fig. S1c) though not in Mn distribution (data not presented). Although mapping
263 was conducted on-the-fly in the horizontal direction with a dwell of 1 ms per virtual 0.1-mm step,
264 damage occurred in a previous study at ends of the horizontal scan lines because of the increased
265 dwell of discrete steps in the vertical direction. In contrast to the effects observed in this previous
266 XANES imaging study, the preliminary experiment in the present study produced no evidence of
267 radiation damage or dehydration to a cowpea leaf after scanning for *c*. 2 h (Fig. 1). This was attributed
268 to the newly-implemented Rascan system which markedly reduced overheads, and hence reduced
269 dwell at the end of the horizontal lines during the vertical move to the next line. We therefore
270 concluded that rapid scanning prevented leaf damage suggesting that experimental artifacts would not
271 arise with time-resolved μ-XRF scans of living leaf tissues.
272
273 **Changes in elemental distribution and concentration**
274

275 There were no visible symptoms of Mn toxicity on leaves of plants grown for 7 d with the basal 0.2
276 μM Mn in solution (Fig. 1a) but there were a few localized spots of Mn accumulation visible in the μ-
277 XRF scans of the detached unifoliate leaf during the preliminary experiment (Fig. 1b,c). This was
278 evident also at 0 h in both living cowpea unifoliate leaves (Fig. 3) but it was only after 2 d at 30 μM
279 Mn that dark spots indicative of Mn accumulation were visible (Fig. 2c).
280 Visual assessment of the detailed μ-XRF scans (Fig. 3) indicated a slight increase over time in
281 the number of high-Mn spots at 0.2 μM Mn, but this increase was considerably lower than that with
282 30 μM Mn in solution. Given that each detailed scan was *c*. 8.5 megapixels, we selected a small area
283 of the image of 1.56 mm^2 (2.6 × 0.6 mm) to examine changes in elemental distribution in the 30-μM
284 Mn treatment over the 48-h experimental period. At the start of the experiment, high Mn spots were
285 visible to the left of the image, the largest being *c*. 240 × 130 μm in size (Fig. 4). Elsewhere, Mn was
286 minimally above background. There was little change in Mn distribution after 6 h at 30 μM Mn, with
287 some new high Mn spots evident after 12 h and especially from 18 to 48 h. Transects across the
288 images from 0 to 48 h (Fig. 4) showed no visible increase in the number or concentration of high Mn
289 spots at 6 h, a few instances where new high Mn spots were visible at 12 h. It was only from 18 to 48
290 h, however, that there were clear increases in spot numbers and in their Mn concentration.
291 As demonstrated by Scheckel *et al*. (2004), ImageJ analysis of the high-resolution data at 30
292 μM Mn (Fig. 4) extended the two-dimensional μ-XRF scans to a three-dimensional geometry
293 providing visual images of both Mn distribution and concentration over the 48-h experimental period
294 (Fig. 5). As with the two-dimensional images (Figs 3, 4), there were a few spots of high Mn at the
295 start of the experiment with no discernable increase at 6 h. It appeared that the number and
296 concentration of Mn in these spots started to increase at 12 h followed by a further increase at 18 h
297 and marked increases at 24 h and 48 h.
298 Using the detailed scan areas of 55.2 and 56.4 mm^2 at 0.2 and 30 μM Mn (Fig. 3), we used
299 ImageJ to calculate the number of localized Mn spots at 0 h was 3.6 and 12.1 mm^{-2} in the two leaves
300 to be subjected to the 0.2 and 30 μM Mn treatments (Fig. 6a). The number of high-Mn spots appeared
301 unchanged over the first 6 h in both treatments. There was a slight increase over 48 h of 4 mm^{-2} at 0.2
302 μM Mn compared to the large increase of 30 mm^{-2} at 30 μM Mn. The corresponding increases in the
303 total area of localized high-Mn spots were < 0.001 and 0.04 mm^2 mm^{-2} (Fig. 6b). Further analyses
304 using ImageJ determined that most of the initial high Mn spots were < 320 μm^2 in size (Fig. S2),
305 largely remaining so over 48 h at 0.2 μM Mn. This contrasted to the changes in spot size in the 30
306 μM-Mn treatment in which the percentage of spots < 64 μm^2 decreased over 48 h. Interestingly, the
307 percentage of slightly larger spots of 64 to < 320 μm increased and then decreased and there was a
308 concomitant increase in large spots at 48 h.
309 With the μ-XRF scans providing quantitative, true-elemental data (Ryan & Jamieson, 1993;
310 Ryan, 2000), GeoPIXE analysis of the detailed μ-XRF scan of leaf sections at 48 h (Fig. 3)
311 determined mean values of 26 and 56 mg Mn kg^{-1} FM at 0.2 and 30 μM Mn. Analysis of the six

transects resulted in a calculated mean Mn concentration that increased from 35 to 61 mg kg^{-1} FM over 48 h exposure to 30 µM Mn (Table S1). However, these transects indicated that the background Mn concentration was < 100 mg kg^{-1} FM other than in the relatively few instances in which the Mn concentration approached or exceeded 1,000 mg kg^{-1} FM. Separating the data into two classes, above and below an estimated background value of 60 mg kg^{-1} FM, permitted further examination of leaf Mn status. Pixel clusters with values < 60 mg Mn kg^{-1} FM had a mean concentration of 24 mg Mn kg^{-1} FM over 48 h, markedly lower than in those with values > 60 mg kg^{-1} FM that increased from 200 to 420 mg Mn kg^{-1} over 48 h (Table S1). Data from the 2.6 × 0.6 mm area used also to determine leaf Mn concentration increased from a mean of 69 to 170 mg kg^{-1} FM over 48 h (Table S1). These estimates differed somewhat from the the bulk Mn concentration in entire unifoliate leaves 48 h after imposing the high Mn treatment of 11 ± 1 and 47 ± 14 mg kg^{-1} FM at 0.2 and 30 µM Mn. (Corresponding values were 80 ± 6 and 360 ± 110 mg kg^{-1} DM.)

Finally, we utilized the µ-XRF analyses at 0 and 48 h to generate images for multiple elements within the energy range of the beamline. In this exercise, the incident X-rays of 12.9 keV and the Maia detector permitted investigation of the distributions and concentrations of elements between P and Zn. (Selection of a higher incident energy would also permit analyses of heavier elements.) The present study permitted investigation of six elements, K, Ca, Mn, Fe, Cu, and Zn, in unifoliate leaves that were above background concentrations (Fig. S3). At 0 h, there was relatively even distribution of K and Ca across the leaves of plants at 0.2 µM Mn, as was that of Cu though at a concentration close to the detection limit. In contrast, Mn and Fe accumulated in localized areas across the leaf, but these elements were not co-located. Localized areas of high Zn were present in and adjacent to the veins. The distributions of these elements were similar 48 h later at 0.2 µM Mn but the distribution of Mn differed between the 0.2 and 30 µM Mn treatments as is evident in Fig. 3.

Discussion

The analysis of fresh tissues exacerbates the many challenges in µ-XRF scanning of low metal and metalloid concentrations in biological tissues (Lombi *et al.*, 2011a). These challenges arise from tissue hydration (often > 85 %) and the generally low concentrations of trace elements in tissues that result in the consequent long transit times required for analysis. A high (long) dwell increases the likelihood of radiation damage and tissue dehydration, thereby resulting in experimental artifacts that affect element distribution (Lombi *et al.*, 2011a). The benchtop (i.e. non-synchrotron based) µ-XRF method developed by Fittschen *et al*. (2017) ensured high sensitivity and low detection limits but required dwells of 1 s per 40 × 40 µm pixel that resulted in substantial radiation damage to a scanned *Arabidopsis thaliana* leaf. Scheckel *et al*. (2004) also noted that µ-XRF analysis using a 1-s dwell of a 6-µm pixel damaged leaves of living *Iberis intermedia* plants. As with these studies, our previous unpublished work showed radiation damage and leaf dehydration was evident in a soybean leaf

349 subjected to multiple scanning (Fig. S1). Recent years, however, have seen major improvements in
350 overcoming these problems in synchrotron-based studies. This has been important in the study of
351 fresh, hydrated root (Kopittke *et al.*, 2011) and leaf tissues (Blamey *et al.*, 2015). Besides the high
352 spatial resolution of 0.1 to 0.2 μm at the Australian Synchrotron XFM beamline (Paterson *et al.*,
353 2011), there are inherent advantages of the Maia detector and Rascan in decreasing dwell. This was
354 evident in the preliminary experiment of the present study in which there was no visible X-ray
355 damage to a unifoliate cowpea leaf after two survey scans and four detailed scans with a combined
356 period of *c*. 2 h (Fig. 1). The recently updated raster scanning adds further advantages by decreasing
357 the damage to sensitive plant tissues.
358 Progress in μ-XRF analysis of hydrated plant tissues has been extended to leaf tissues of
359 living plants. For example, by growing the hyperaccumulator *I. intermedia* plants at elevated Tl in
360 soil, Scheckel *et al*. (2004) determined that Tl accumulated mostly in the vascular tissues. Fittschen *et*
361 *al*. (2017) constructed a benchtop μ-XRF unit to examine differences in the distributions of a number
362 of nutrients in the vascular system, mesophyll, and trichomes of leaves of living *A. thaliana* plants.
363 These studies, however, did not investigate time-resolved changes in elemental distribution and
364 concentration and we were not able to find instances in the literature of sequential μ-XRF analysis of
365 living plant tissues.
366 In the present study, μ-XRF detailed scans using a pixel size of 4 × 4 μm enabled production
367 of high-quality images that permitted direct visual comparisons between the effects of 0.2 and 30 μM
368 Mn (Fig. 3) and enabled high resolution comparisons of Mn accumulation of 30 μM Mn over 48 h
369 (Fig. 4). A pixel size of 1 × 1 μm allows even better resolution where appropriate (Blamey *et al.*,
370 2015). As demonstrated by Scheckel *et al*. (2004) and in the present study (Fig. 5), three-dimensional
371 representations of the two-dimensional scans provide further visualization of elemental distribution
372 and concentration.
373 Until recently, quantitative elemental analyses have focused on bulk tissues, from whole
374 plants to separate analyses of roots, shoots, stems, and leaves (Salt *et al.*, 2008) but technological
375 developments in synchrotron-based μ-XRF, amongst other techniques, provide greater spatial
376 resolution of the ionome (Punshon *et al.*, 2009; van der Ent *et al.*, 2017). However, van der Ent *et al*.
377 (2017) urged caution in the use of μ-XRF in foliar studies using living plants because measurements
378 arise from different depths, from different cell types (e.g., epidermis, palisade, mesophyll, and
379 vasculature), and from continued plant metabolism. The first two of these potential difficulties may be
380 addressed by a combination of analytical techniques as shown by Blamey *et al*. (2017) who used
381 NanoSIMS to confirm the suspected accumulation of Mn in the apoplast using μ-XRF by analysis.
382 The present study has also shown that accommodation of continued plant metabolism is possible,
383 albeit in only one instance of Mn accumulation. High Mn accumulation in discreet locations is of
384 additional benefit by overcoming the overall low concentrations of many trace elements.

385 It has been recognized for many years that symptoms of Mn toxicity precede a decrease in
386 plant growth (Foy *et al.*, 1978; Weil *et al.*, 1997), information extended by Fernando *et al*. (2016)
387 with Mn accumulation in leaves of wheat (*Triticum aestivum*) plants well before the appearance of
388 visible symptoms. This was evident in leaves of cowpea exposed to a non-toxic concentration of 0.2
389 μM Mn (Figs 1, 3, 4, 5). Localized spots of high Mn preceded visible symptoms associated with Mn
390 toxicity in the present study also with new high Mn spots first visible after 12 h growth at 30 μM Mn
391 (Figs 4, 5) but visible dark spots appeared only after 48 h (Fig. 2c). However, the mechanism is
392 unknown whereby high Mn accumulates in specific localized areas not visibly associated with leaf
393 anatomy (e.g., close to or distant from veins). There is similar uncertainty as to why an overall
394 increase in Mn in leaf tissues at 30 μM Mn (Figs 4 and 5) results in localized increases in Mn but no
395 general increase in background Mn concentration over time.
396 From an ionomics viewpoint (Salt *et al.*, 2008), the present study addressed various
397 microscopic measures of Mn concentration in leaf tissues based on the true-elemental data of the μ-
398 XRF scans. After 48 h at 0.2 μM Mn, these analyses ranged from 24 to 35 mg Mn kg^{-1} FM compared
399 to the unifoliate leaf bulk analysis of 11 mg Mn kg^{-1} FM. The corresponding comparison was 56 to
400 169 mg kg^{-1} versus a bulk leaf tissue concentration of 47 mg Mn kg^{-1} FM at 30 μM Mn. While of the
401 same order of magnitude, these findings suggest that further research is required in the sampling for
402 quantitative determination of elemental concentrations in leaf tissues. Importantly, the multi-element
403 analyses undertaken in the present study would provide important information on interactions
404 between the various elements. An example relevant to the present study might use detailed μ-XRF
405 studies to examine the kinetics of changes in Mn distribution (Figs 4, 5) with those of Ca (Fig. S3)
406 given the role of Ca in callose formation associated with Mn toxicity (Wissemeier & Horst, 1987).
407 Additional studies may also provide critical information as to the underlying mechanisms whereby
408 Mn is toxic by determining changes in Ca and Mn accumulation in the apoplast and by determining
409 how Mn accumulates along with Ca in vacuoles of some plant species but not in others. Finally, there
410 is particular promise in studies such as that by Takahashi *et al*. (2009) in combining information on
411 the activities of metal transporter genes with multi-element μ-XRF analysis of changes in the
412 distribution of Fe, Mn, Cu, and Zn in germinating rice (*Oryza sativa*) seeds.
413
414 **Conclusion**
415
416 Development of a synchrotron-based method has shown the feasibility of using μ-XRF analysis to
417 determine the distribution and concentration of Mn in living unifoliate leaves of cowpea exposed to
418 0.2 and 30 μM Mn in solution culture. This method may be adapted to examine the accumulation and
419 distribution of other elements and plant species over a range in exposure times. Besides investigations
420 of elemental toxicities, other examples may include determining the dynamics of nutrients upon

addition to a nutrient-deficient plant, the effects of hypoxia on nutrient status, and establishing the relationship between transpiration and nutrient accumulation in leaf tissues.

The results and implications of the present study advance the value of ionomics, the inorganic component of the metabolome, through quantifying changes in the microscopic distribution and concentration of elements *in vivo* (Salt *et al.*, 2008). Though focusing the present study on the kinetics of Mn accumulation in cowpea unifoliate leaves, μ-XRF analyses may also provide multi-element information in plant tissues, meeting an aim of ionomics to define the functional state of an organism driven by genetic, developmental, biotic, or abiotic influences.

Acknowledgements

F.P.C.B. acknowledges assistance from the Australian Government Research Training Program and P.M.K. acknowledges receipt of an Australian Research Council (ARC) Future Fellowship (FT120100277). This research was undertaken on the XFM beamline (Project AS153/XFM/11040) at the Australian Synchrotron, part of the Australian Nuclear Science and Technology Organization (ANSTO). We thank Dr Chris Ryan (CSIRO), Dr Martin de Jonge, and Dr Daryl Howard (Australian Synchrotron) for assistance with synchrotron-based techniques.

Author contributions

F.P.C.B. conceived the research program that was developed in collaboration with D.J.P., A.W., N.W.M., and P.M.K.; A.W. and N.A. developed the requisite technology; F.P.C.B., M.C., and C.T. conducted the plant growth experiments; F.P.C.B., D.J.P., B.A.M., M.C., and P.M.K. conducted the μ-XRF analyses at the Australian Synchrotron; F.P.C.B and P.M.K. analyzed the data; and F.P.C.B., D.J.P, and P.M.K. wrote the first draft of the article to which all authors contributed.

448 **References**

449 **Babourina O, Rengel Z. 2009.** Uptake of aluminium into *Arabidopsis* root cells measured by
450 fluorescent lifetime imaging. *Annals of Botany* **104**: 189-195.

451 **Blamey FPC, Hernandez-Soriano MC, Cheng M, Tang C, Paterson DJ, Lombi E, Wang WH,**
452 **Scheckel KG, Kopittke PM. 2015.** Synchrotron-based techniques shed light on mechanisms
453 of plant sensitivity and tolerance to high manganese in the root environment. *Plant*
454 *Physiology* **169**: 2006-2020.

455 **Blamey FPC, McKenna BA, Li C, Cheng M, Tang C, Jiang H, Howard DL, Paterson DJ,**
456 **Kappen P, Wang P*, et al.* 2017.** Manganese distribution and speciation help to explain the
457 effects of silicate and phosphate on manganese toxicity in four crop species. *New Phytologist*.
458 doi: 10.1111/nph.14878.

459 **Bravo P, Uribe EG. 1981.** Temperature dependence of the concentration kinetics of absoprtion of
460 phosphate and potassium in corn roots. *Plant Physiology* **67**: 815-819.

461 **Conn S, Gilliham M. 2010.** Comparative physiology of elemental distributions in plants. *Annals of*
462 *Botany* **105**: 1081-1102.

463 **Cosio C, DeSantis L, Frey B, Diallo S, Keller C. 2005.** Distribution of cadmium in leaves of *Thlaspi*
464 *caerulescens*. *Journal of Experimental Botany* **56**: 765-775.

465 **Danilatos GD. 1981.** The examination of fresh or living plant material in an environmental scanning
466 electron microscope. *Journal of Microscopy* **121**: 235-238.

467 **Fernando DR, Moroni SJ, Scott BJ, Conyers MK, Lynch JP, Marshall AT. 2016.** Temperature
468 and light drive manganese accumulation and stress in crops across three major plant families.
469 *Environmental and Experimental Botany* **132**: 66-79.

470 **Fittschen UEA, Kunz HH, Hohner R, Tyssebotn IMB, Fittschen A. 2017.** A new micro X-ray
471 fluorescence spectrometer for *in vivo* elemental analysis in plants. *X-Ray Spectrometry* **46**:
472 374-381.

473 **Foy CD, Chaney RL, White MC. 1978.** The physiology of metal toxicity in plants. *Annual Review*
474 *of Plant Physiology* **29**: 511-566.

475 **Heenan DP, Carter OG. 1976.** Tolerance of soybean cultivars to manganese toxicity. *Crop Science*
476 **16**: 389-391.

477 **Hevesy G. 1923.** The absorption and translocation of lead by plants. A contribution to the application
478 of the method of radioactive indicators in the investigation of the change of substance in
479 plants. *Biochemical Journal* **17**: 439-445.

480 **Horst WJ. 1983.** Factors responsible for genotypic manganese tolerance in cowpea (*Vigna*
481 *unguiculata*). *Plant and Soil* **72**: 213-218.

482 **Jahnke S, Menzel MI, van Dusschoten D, Roeb GW, Buhler J, Minwuyelet S, Blumler P,**
483 **Temperton VM, Hombach T, Streun M*, et al.* 2009.** Combined MRI-PET dissects dynamic
484 changes in plant structures and functions. *Plant Journal* **59**: 634-644.

485 **Kopittke PM, Blamey FPC, Asher CJ, Menzies NW. 2010.** Trace metal phytotoxicity in solution
486 culture: A review. *Journal of Experimental Botany* **61**: 945-954.
487 **Kopittke PM, Lombi E, McKenna BA, Wang P, Donner E, Webb RI, Blamey FPC, de Jonge**
488 **MD, Paterson D, Howard DL*, et al.* 2013.** Distribution and speciation of Mn in hydrated
489 roots of cowpea at levels inhibiting root growth. *Physiologia Plantarum* **147**: 453-464.
490 **Kopittke PM, Menzies NW, de Jonge MD, McKenna BA, Donner E, Webb RI, Paterson DJ,**
491 **Howard DL, Ryan CG, Glover CJ*, et al.* 2011.** In situ distribution and speciation of toxic
492 copper, nickel, and zinc in hydrated roots of cowpea. *Plant Physiology* **156**: 663-673.
493 **Kopittke PM, Moore KL, Lombi E, Gianoncelli A, Ferguson BJ, Blamey FPC, Menzies NW,**
494 **Nicholson TM, McKenna BA, Wang P*, et al.* 2015.** Identification of the primary lesion of
495 toxic aluminum in plant roots. *Plant Physiology* **167**: 1402-1411.
496 **Lombi E, de Jonge MD, Donner E, Kopittke PM, Howard DL, Kirkham R, Ryan CG, Paterson**
497 **D. 2011a.** Fast X-ray fluorescence microtomography of hydrated biological samples. *PLoS*
498 *ONE* **6**: 1-5.
499 **Lombi E, Smith E, Hansen TH, Paterson D, de Jonge MD, Howard DL, Persson DP, Husted S,**
500 **Ryan C, Schjoerring JK. 2011b.** Megapixel imaging of (micro)nutrients in mature barley
501 grains. *Journal of Experimental Botany* **62**: 273-282.
502 **Lombi E, Susini J. 2009.** Synchrotron-based techniques for plant and soil science: opportunities,
503 challenges and future perspectives. *Plant and Soil* **320**: 1-35.
504 **McGregor JE, Donald AM 2010.** The application of ESEM to biological samples. In: Baker RT ed.
505 *Electron Microscopy and Analysis Group Conference 2009*, 012021.
506 **McNear DH, Peltier E, Everhart J, Chaney RL, Sutton S, Newville M, Rivers M, Sparks DL.**
507 **2005.** Application of quantitative fluorescence and absorption-edge computed
508 microtomography to image metal compartmentalization in *Alyssum murale*. *Environmental*
509 *Science & Technology* **39**: 2210-2218.
510 **McNear DHJ, Küpper JV. 2014.** Mechanisms of trichome-specific Mn accumulation and toxicity in
511 the Ni hyperaccumulator *Alyssum murale*. *Plant and Soil* **377**: 407-422.
512 **Moore KL, Chen Y, van de Meene AML, Hughes L, Liu WJ, Geraki T, Mosselmans F,**
513 **McGrath SP, Grovenor C, Zhao FJ. 2014.** Combined NanoSIMS and synchrotron X-ray
514 fluorescence reveal distinct cellular and subcellular distribution patterns of trace elements in
515 rice tissues. *New Phytologist* **201**: 104-115.
516 **Paterson DJ, de Jonge MD, McKinlay WLJ, Starritt A, Kusel M, Ryan CG, Kirkham R,**
517 **Moorhead G, Siddons DP. 2011.** The X-ray fluorescence microscopy beamline at the
518 Australian synchrotron. *AIP Conference Proceedings* **1365**: 219-222.
519 **Punshon T, Guerinot ML, Lanzirotti A. 2009.** Using synchrotron X-ray fluorescence microprobes
520 in the study of metal homeostasis in plants. *Annals of Botany* **103**: 665-672.

521 **Ryan CG. 2000.** Quantitative trace element imaging using PIXE and the nuclear microprobe.
522 *International Journal of Imaging Systems and Technology* **11**: 219-230.
523 **Ryan CG, Jamieson DN. 1993.** Dynamic analysis: on-line quantitative PIXE microanalysis and its
524 use in overlap-resolved elemental mapping. *Nuclear Instruments & Methods in Physics*
525 *Research Section B-Beam Interactions with Materials and Atoms* **77**: 203-214.
526 **Salt DE, Baxter I, Lahner B. 2008.** Ionomics and the study of the plant ionome. *Annual Review of*
527 *Plant Biology* **59**: 709-733.
528 **Scheckel KG, Lombi E, Rock SA, McLaughlin MJ. 2004.** In vivo synchrotron study of thallium
529 speciation and compartmentation in *lberis intermedia*. *Environmental Science & Technology*
530 **38**: 5095-5100.
531 **Schneider CA, Rasband WS, Eliceiri KW. 2012.** NIH Image to ImageJ: 25 years of image analysis.
532 *Nature Methods* **9**: 671-675.
533 **Solon EG, Schweitzer A, Stoeckli M, Prideaux B. 2010.** Autoradiography, MALDI-MS, and SIMS-
534 MS imaging in pharmaceutical discovery and development. *The AAPS Journal* **12**: 11-26.
535 **Sugita R, Kobayashi NI, Hirose A, Saito T, Iwata R, Tanoi K, Nakanishi TM. 2016.** Visualization
536 of uptake of mineral elements and the dynamics of photosynthates in Arabidopsis by a newly
537 developed real-time radioisotope imaging system (RRIS). *Plant and Cell Physiology* **57**: 743-
538 753.
539 **Takahashi M, Nozoye T, Kitajima N, Fukuda N, Hokura A, Terada Y, Nakai I, Ishimaru Y,**
540 **Kobayashi T, Nakanishi H*, et al.* 2009.** In vivo analysis of metal distribution and expression
541 of metal transporters in rice seed during germination process by microarray and X-ray
542 Fluorescence Imaging of Fe, Zn, Mn, and Cu. *Plant and Soil* **325**: 39-51.
543 **Tsukamoto T, Nakanishi H, Kiyomiya S, Watanabe S, Matsuhashi S, Nishizawa NK, Mori S.**
544 **2006.** ^{52}Mn translocation in barley monitored using a positron-emitting tracer imaging system.
545 *Soil Science and Plant Nutrition* **52**: 717-725.
546 **van der Ent A, Przybyłowicz WJ, de Jonge MD, Harris HH, Ryan CG, Tylko G, Paterson DJ,**
547 **Barnabas AD, Kopittke PM, Mesjasz-Przybyłowicz J. 2017.** X-ray elemental mapping
548 techniques for elucidating the ecophysiology of hyperaccumulator plants. *New Phytologist*.
549 doi: 10.1111/nph.14810.
550 **Walczysko P, Wagner E, Albrechtova JTP. 2000.** Use of co-loaded Fluo-3 and Fura Red
551 fluorescent indicators for studying the cytosolic Ca^{2+} concentrations distribution in living
552 plant tissue. *Cell Calcium* **28**: 23-32.
553 **Weil RR, Foy CD, Coradetti CA. 1997.** Influence of soil moisture regimes on subsequent soil
554 manganese availability and toxicity in two cotton genotypes. *Agronomy Journal* **89**: 1-8.
555 **Wissemeier AH, Horst WJ. 1987.** Callose deposition in leaves of cowpea (*Vigna unguiculata* (L.)
556 Walp.) as a sensitive response to high Mn supply. *Plant and Soil* **102**: 283-286.
557

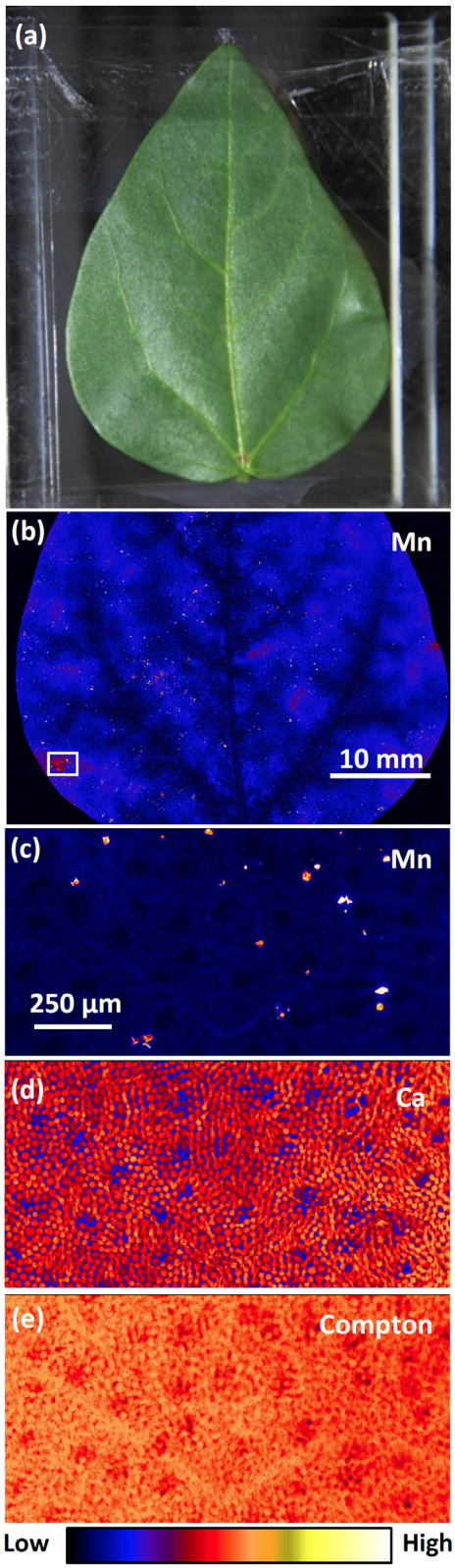

Fig. 1. Images of a detached unifoliate leaf of cowpea grown for 7 d at 0.2 µM Mn after conducting a survey scan and three detailed scans. (a) Optical image of a leaf mounted between Ultralene® films. (b) Survey µ-XRF scan of Mn distribution, the white box showing the area of subsequent detailed scans. (c,d) Detailed µ-XRF scan showing the distributions of Mn and Ca. (e) Detailed Compton scatter.

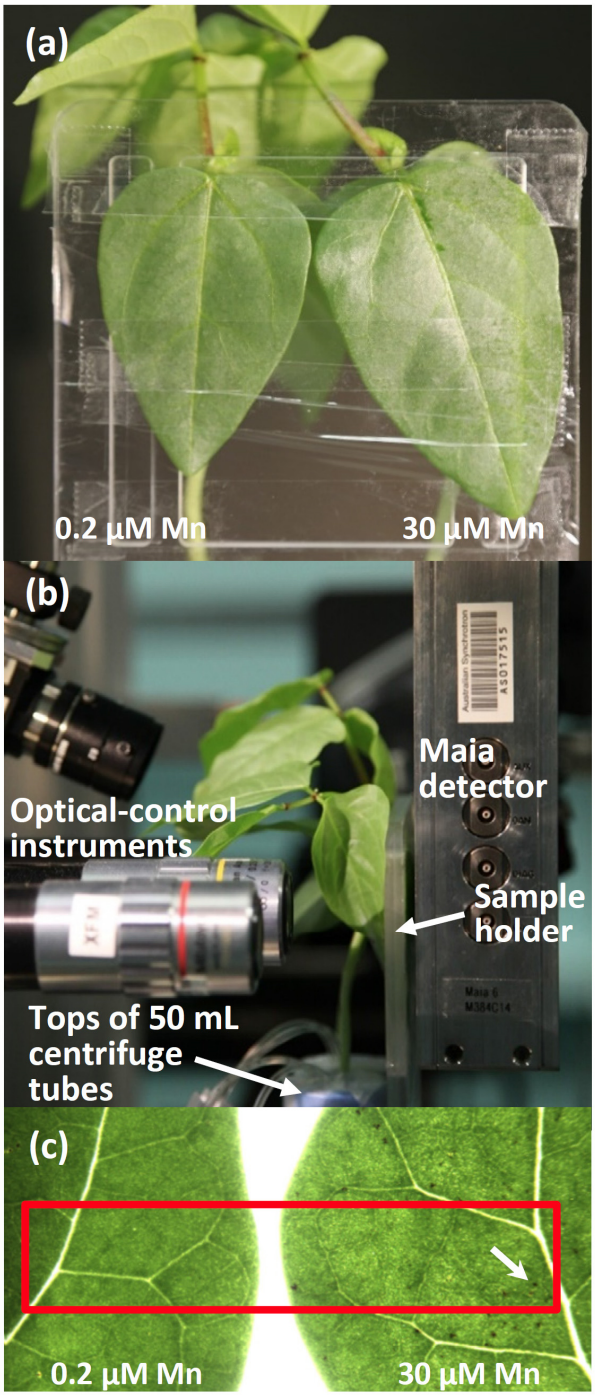

Fig. 2. Optical images of cowpea unifoliate leaf arrangement in the sample holder. (a) Leaves of two plants grown at 0.2 and 30 µM Mn between Ultralene® films in the sample holder. (b) Arrangement of living plants mounted in the X-ray beam. (c) Micrograph of unifoliate leaves after the detailed µ-XRF scan at 48 h, the red box showing the area of sequential detailed scans and the white arrow a visible dark spot of Mn accumulation at 30 µM Mn.

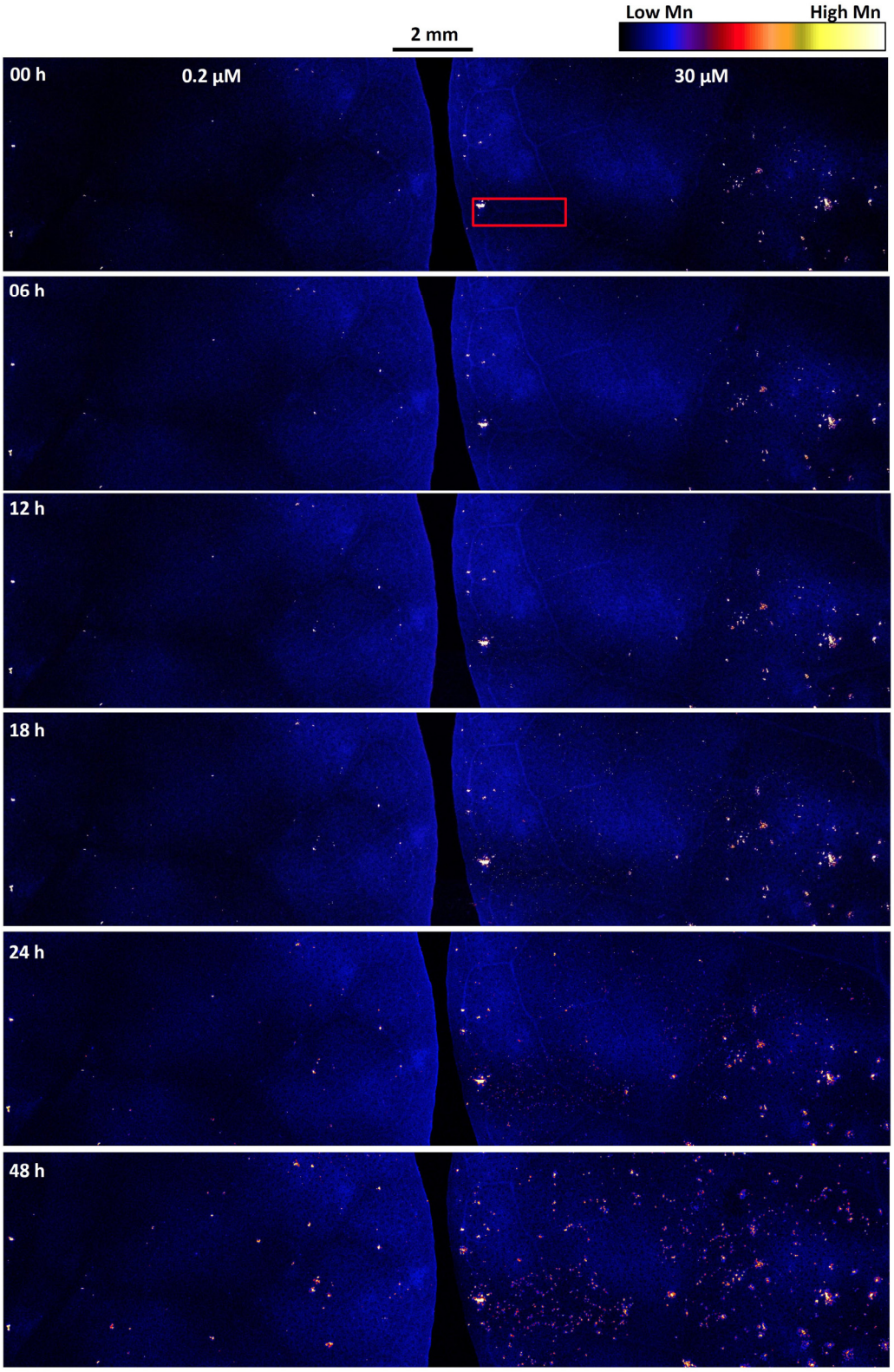

Fig. 3. Detailed µ-XRF scans of Mn distribution in unifoliate leaves of cowpea from 0 to 48 h after initial exposure to 30 µM Mn in solution culture. The red box at 0 h shows the area analyzed at high resolution for the distribution of Mn (Fig. 4), for three-dimensional representation of Mn distribution and concentration (Fig. 5), and for ImageJ and GeoPIXE analyses (Fig. 6).

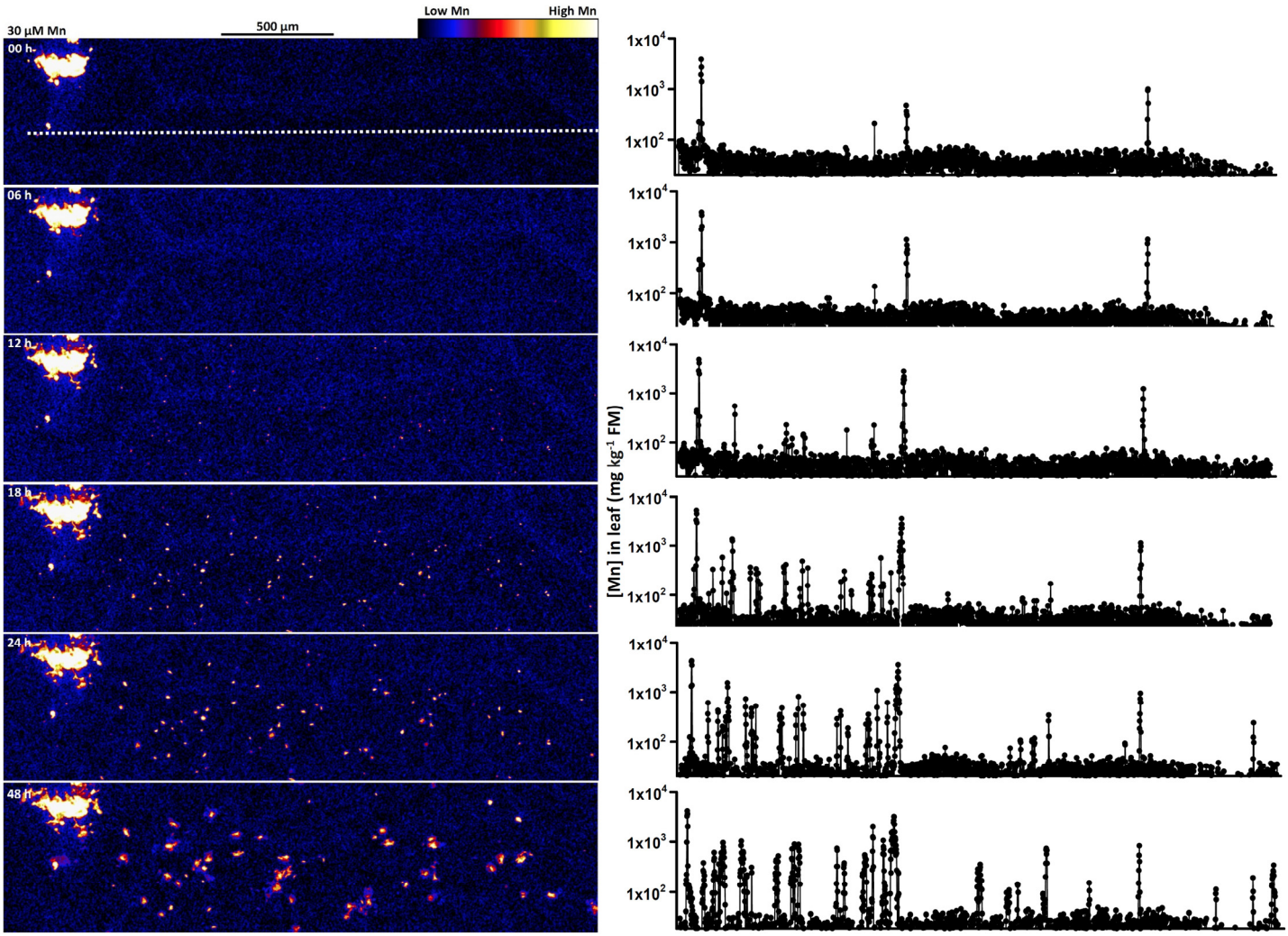

Fig. 4. High-resolution µ-XRF scans and transects of Mn distribution and concentration (log_{10} scale) from 0 to 48 h after initial exposure to 30 µM Mn in a 2.6 mm × 0.6 mm section of a cowpea unifoliate leaf (Fig. 3). The horizontal dotted line at 0 h identifies the position of transects along which the concentration of Mn was determined.

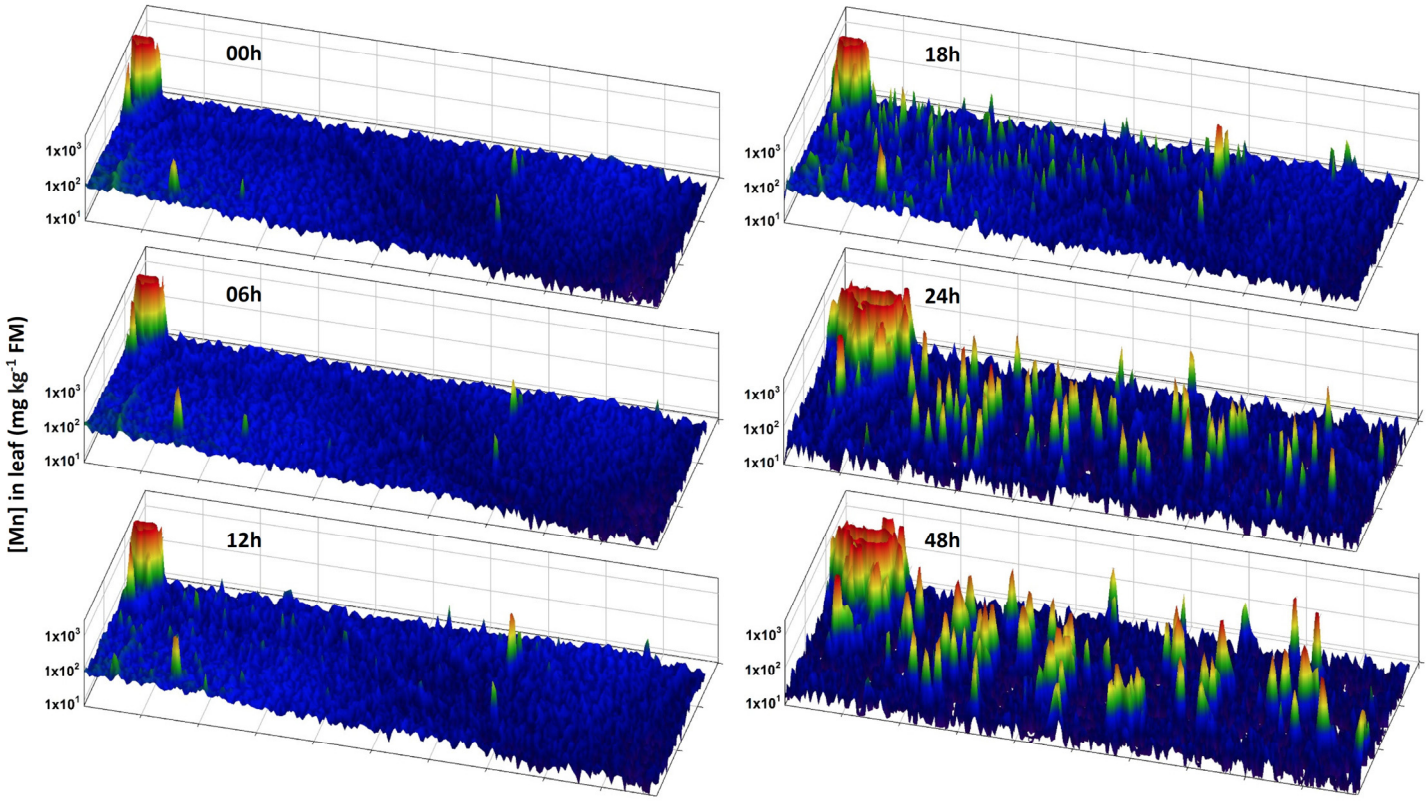

Fig. 5. Three-dimensional representation of Mn distribution and concentration in unifoliate leaf sections of cowpea from 0 to 48 h after initial exposure to 30 µM Mn. The scanned area is 2.6 mm × 0.6 mm as shown by the red box in Fig. 3 and the high-resolution µ-XRF images in Fig. 4. The Mn concentration in the large high-Mn spot (back left) exceeded 10,000 mg kg^{-1} FM from 0 to 48 h but the scale of Mn in the unifoliate leaf has been limited to 1,000 mg kg^{-1} FM to show the change in high Mn spots that developed during the 48-h experimental period.

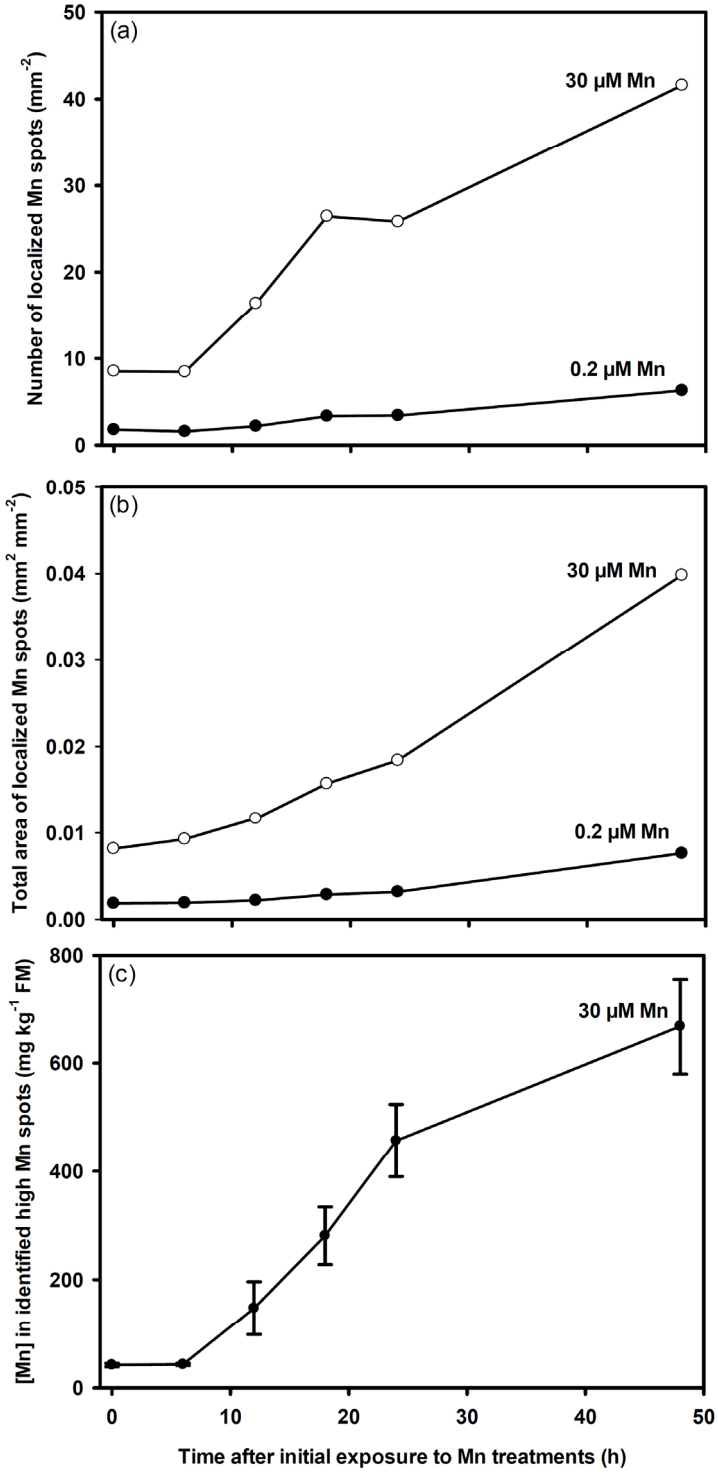

Fig. 6. Accumulation of Mn in unifoliate leaf sections (Fig. 3) of cowpea from 0 to 48 h after initial exposure to 30 µM Mn in solution culture. (a,b) ImageJ determination of the number and area of localized spots of high Mn in detailed scans of leaf sections (Fig. 3). (c) GeoPIXE determination of the Mn concentration in identified high Mn spots (i.e. > 60 mg kg^{-1} FM) over 48 h in transects of the section of a cowpea unifoliate leaf at 30 µM Mn (Fig. 4).